J. Membrane Biol. 178, 21–30 (2000)
DOI: 10.1007/s002320010011

The Journal of
Membrane
Biology

Calcium Channel Current in Rat Dental Pulp Cells

R.M. Davidson[1,2], **L. Guo**[1]
[1]Division of Basic Sciences, 345 East 24th Street, New York University College of Dentistry, New York, NY 10010-4087, USA
[2]Department of Periodontics, New York University College of Dentistry, New York, NY 10010-4087, USA

Received: 29 November 1999/Revised: 24 April 2000

Abstract. Voltage-gated Ca^{2+} currents in early-passage rat dental pulp cells were studied using whole-cell patch-clamp techniques. With Ba^{2+} as the charge carrier, two prominent inwardly-directed currents, I_f and I_s, were identified in these cells that could be distinguished on the basis of both kinetics and pharmacology. I_f was activated by membrane depolarizations more positive than −30 mV, and displayed fast inactivation kinetics, while I_s was activated by steeper depolarizations and inactivated more slowly. At peak current, time constants of inactivation for I_f and I_s were ~17 *vs.* ~631 msec. Both I_f and I_s could be blocked by lanthanum. By contrast, only I_s was sensitive to either Bay-K or nifedipine, a specific agonist and antagonist, respectively, of L-type Ca^{2+} channels. I_s was also blocked by the peptide omega-Conotoxin GVIA. Taken together, results suggested that I_f was mediated by divalent cation flow through voltage-gated T-type Ca^{2+} channels, whereas I_s was mediated by L- and N-type Ca^{2+} channels in the pulp cell membrane. The expression of these prominent, voltage-gated Ca^{2+} channels in a presumptive mineral-inductive phenotype suggests a functional significance *vis a vis* differentiation of dental pulp cells for the expression and secretion of matrix proteins, and/or formation of reparative dentin itself.

Key words: Dental pulp — Ca^{2+} current — Dihydropyridine — Lanthanum — Conotoxin — In vitro

Introduction

Dental pulp fibroblasts represent a heterogeneous group of cells that resides within the pulp chamber of mammalian teeth surrounded by a specialized form of mineralized tissue, i.e., dentin. These cells are thought to play a pivotal role in the type of mineral induction, i.e., dentinogenesis, that represents a protective response of the dental pulp to injury. That is, the response to certain pathophysiological cues results in (i) their differentiation into mineral-producing cells [20, 27, 31] and (ii) the active deposition of mineralized tissue in the form of secondary dentin [1, 19, 33]. Although the cellular mechanisms underlying both differentiation and dentin formation by pulp cells are as yet unclear, calcium mobilization and transport are thought to be foundational steps in this process [18, 35].

For mineral-inductive cells, in particular, ionic calcium is perhaps the most critical factor in regulation of the process of mineralization [6, 9, 23], since it serves not only as a second-messenger mediating intracellular signal transduction, but also as a structural component in the apatite crystal itself [22]. In previous studies, we have identified several classes of K^+ channel and one neural-like Na^+ current in cells derived from human dental pulp [4, 5]. These findings suggested that dental pulp cells were electrophysiologically more active than might be expected for nonexcitable connective tissue cells. In the present study, in order to gain mechanistic insight into regulation of calcium homeostasis and transport by dental pulp cells, we examined two very prominent voltage-gated Ca^{2+} channel currents in this interesting phenotype.

Materials and Methods

Isolation and Maintenance of Dental Pulp Cells

All animal care and use protocols were approved by the New York University Animal Welfare Committee. Dental pulp cells were isolated from adult Sprague-Dawley rats of either sex (200–400 g) by a method modified from previous experiments using rat odontoblasts

Correspondence to: R.M. Davidson

[15, 16] and from Kasugai et al. [19] and Nakashima [24]. For each preparation, following sacrifice of the animal with CO_2, incisor teeth were removed and submerged in sterile phosphate-buffered saline (PBS). After removing all visible connective tissue and bone fragments adhering to the outside of the tooth, teeth were submerged in 70% (v/v) ethanol for 2 min and then rinsed twice with PBS. Next, teeth were split with a scalpel blade, and the pulpal connective tissue was removed with fine forceps and moved to a 10-cm culture dish containing 2 ml of ECS (*see* below) with 0.02% trypsin. The pulp was minced and then incubated at 37°C for 30 min. Following incubation, 2 ml of Dulbecco's modified Eagle's minimum essential medium (DMEM, Cellgro, Mediatech, Herndon, VA) supplemented with 10% (v/v) Fetal Bovine Serum (FBS, Cellgro), 100 IU/ml penicillin, 100 μg/ml streptomycin and 0.25 μg/ml amphotericin B was added to the dish to stop the enzymatic activity. All contents of the dish were transferred to a 15 ml centrifuge tube and the dish was further rinsed with 8 ml more such medium. The dispersed dental pulp cells centrifuged at 200 g for 10 min at 5°C. The pellet was resuspended with 6 ml DMEM plus supplements described above and plated in a 25 cm^2 flask. Cells were maintained in a 5% CO_2-95% air incubator at 37°C. Fresh medium was changed twice a week and cells reached confluence in approximately 1–2 months. From the first passage, antibiotics and antimycotics were excluded from the medium. For these studies, 1st and 2nd passage cells were harvested by trypsin-EDTA treatment (0.25% trypsin, 0.1% EDTA in PBS, Cellgro) and plated on 12 mm #1D glass coverslips (Fisher Scientific, Pittsburgh, PA) at a density of 1~2 × $10^3/cm^2$ and experiments were conducted one day following plating until cells reached confluence.

Electrophysiological Recording

Coverslips with cells were placed in a recording/perfusion chamber (Model P4, Warner Instrument, Hamden, CT), with a volume of 1 ml, that was mounted on an inverted microscope (IMT-2, Olympus, Tokyo) equipped with Hoffman modulation contrast optics (Modulation Optics, Greenvale, NY) or Nomarski differential interference contrast optics (IMT2-NIC, Olympus). Patch pipettes were pulled from borosilicate glass tubing (Microcaps-1000, Drummond Scientific, Broomall, PA) on a multistage P-87 Flaming/Brown microelectrode puller (Sutter Instrument, Novato, CA), coated with silicone elastomer (Sylgard, Down Corning, Midland, MI), then fire-polished on an MF-84 microforge (Narishige, Tokyo). When filled with pipette solutions, the tip resistance of recording pipettes was 0.8 to 1.8 MΩ. The whole-cell currents were recorded at room temperature using an Axopatch-1C patch clamp amplifier (Axon Instruments, Foster City, CA). Amplified currents were first filtered with an eight-pole low-pass Bessel filter (−3 dB at 1 KHz), then digitized at a sampling rate of 5 KHz and stored on disk for offline analysis. Recording pipette and whole-cell capacitance, and series resistance were corrected by compensation. Whole-cell capacitance and series resistance were estimated by cancellation of the capacitive transient following rupture of the membrane; values for the total of 158 whole-cell patches were 44.1.5 ± 3 pF and 2.8 ± 0.1 MΩ, respectively. Liquid-junction potentials between patch pipette and bath solutions were manually corrected prior to contact with the cell membrane. Leak current was assumed to be linear and was estimated either by extrapolating the inward linear current evoked by hyperpolarizing voltage commands before voltage-gated current was detected, or by completely blocking voltage-gated currents by appropriate channel blockers. Leak current was digitally subtracted offline as indicated. Whole-cell currents were measured during 60 to 360 msec step depolarizations from a holding potential (V_h) of −60 or −80 mV. Depolarizing voltage steps were typically applied in 10 mV increments with a 3-sec interval between each pulse. Voltage step or ramp commands were computer-generated using pCLAMP6 (Axon Instruments), and the same suite of software was used for current recording and offline analysis.

Solutions

Standard extracellular Na^+-rich solution (ECS) was composed of (in mM): 140 NaCl, 3 KCl, 1 $MgCl_2$, 2 $CaCl_2$, 10 HEPES; pH adjusted to 7.35 with NaOH. Although Ca^{2+} current could be occasionally detected in ECS, in order to avoid contamination with Na^+ and K^+ currents in these recordings and to prevent the possible Ca^{2+}-dependent inactivation of Ca^{2+} channels, unless otherwise noted (Figs. 9 and 10), 110 mM isotonic Ba^{2+} external solution was used in all experiments. The Ba^{2+} rich bath solution was composed of: 110 $BaCl_2$, 10 HEPES; pH 7.35. Pipettes were filled with a Cs^+-rich solution containing: 140 CsCl, 1 $MgCl_2$, 2 EGTA, 3 Mg^{2+}-ATP, 10 HEPES; pH adjusted to 7.35 with CsOH.

Preparation and Application of Reagents

$LaCl_3$ was prepared as a 1M stock solution, then diluted into perfusion (extracellular) solutions. Nifedipine and Bay-K were dissolved in dimethylsulfoxide (DMSO) as 50-mM stock solution, stored at −20°C and diluted into extracellular solutions. Tetrodotoxin (TTX) and omega-Conotoxin GVIA (GVIA) were first dissolved in distilled water as 1 mM stock solution and stored in frozen aliquots. Drugs were applied to cells by a multibarrel bath perfusion system. All chemicals in this study were purchased from Sigma (St. Louis, MO).

Statistical Analysis

Data were represented as the Mean ± SEM. Group means were compared using Student's paired or unpaired *t*-test as appropriate, based on a significance level of $P < 0.05$.

Results

Identification of Dental Pulp Fibroblasts

Dental pulp fibroblasts could be distinguished on the basis of morphological criteria. Within the first 96 hr, two predominant phenotypes were seen. The most common comprised ~50–60% of the total cell population. These fibroblastlike cells were ~20–30 μm in diameter, rounded in appearance, had fine branching extending in all directions, i.e., had a stellate appearance, and contacted cells of similar morphology. A second phenotype (~20–30%) were typically large (>60 μm), flattened cells that had indistinct borders. By days 12–14 in culture, subconfluent cells displayed a third general phenotype which had displaced the larger cells. These cells typically grew in discrete colonies, and were of smaller size than the stellate cells. This phenotype comprised ~20% of the total cell population. An additional cell type was a spindlelike cell with a long slender process that constituted ~5–10% of the cell population.

Activation of I_F and I_S

Depolarizing voltage pulses activated a voltage-gated, inward Ba^{2+} current in 96% (108/113) of the fibroblast cells described above. Although characteristics of both currents could be seen in many recordings, in 52% (57/108) of these cells the predominant current displayed rapid inactivation kinetics that resulted in a fast inactivating, i.e., transient, phase (I_f). By contrast, in 31% (33/108) of these cells the predominant current displayed slow inactivation kinetics, characterized by a sustained, i.e., steady-state, phase following depolarization (I_s). In 17% (18/108) of cells, both currents could be seen.

Figure 1(*a* and *b*) illustrates the family of inward Ba^{2+} currents obtained from two cells in which either I_f(*a*) or I_s(*b*) was predominantly expressed. In Fig. 1*a*, depolarizing the cell to a membrane voltage more positive than −30 mV activated an inward current that increased in magnitude with increasing depolarization, reaching peak amplitude at 10 mV. Activation of this current was quite rapid. In this example, the current reached a peak of −257 pA within 6.8 msec. Likewise, current inactivation was quite rapid; in this case, the current decreased to ~30% of its peak value (−77 pA) within 30 msec of reaching peak amplitude. In Fig. 1*b*, inward current was activated in response to depolarizing steps more positive than −20 mV, and reached peak amplitude at 40 mV. Activation of this current was also very fast. Once activated, it took only 8.4 msec to reach peak amplitude. With respect to inactivation, however, and in contrast to the example in Fig. 1*a*, this current displayed negligible decay, decreasing only ~25% from a peak of −297 to −221 pA over the duration of the depolarizing pulse. The current-voltage relation generated from the data in Fig. 1*a* and *b* is shown in Fig. 1*c*. Typically, the peak amplitude of I_s was of greater magnitude than that of I_f. For 57 cells in which I_f was the predominant current, the peak value of I_f was −164 ± 120 pA. By contrast, in 33 cells which expressed mainly I_s, the peak value was −467 ± 66 pA ($P < 0.01$).

Time Constant of Decay of I_F and I_S

Because I_f and I_s displayed significant differences in inactivation kinetics, inactivation time constants were analyzed for cells in which only I_f or I_s was expressed. As shown in Fig. 2*a* and *b*, the inactivation (decaying) phases of both I_f and I_s could be best fitted by a single-exponential equation:

$$I = I_{max}[1-\exp(-t/\tau)] \quad (1)$$

where I is the current magnitude at time t, I_{max} is the peak value, and τ represents the inactivation time constant (τ_{inact}). That both currents showed voltage-dependence

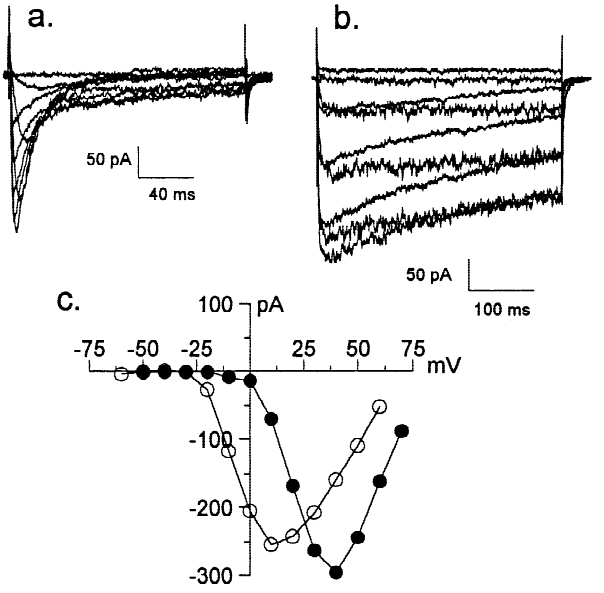

Fig. 1(a–c) Ca^{2+} current in dental pulp cells. (*a*) Typical rapidly inactivating current (I_f) obtained in dental pulp cell held at −60 mV. Depolarizing pulses of 180-msec duration were applied every 3 sec over a range of voltages between −60 to 60 mV with 10-mV increments. For clarity, only selected traces from −30 to 60 mV are shown. (*b*) Typical slowly inactivating current (I_s) obtained from a different preparation. This cell was also held at −60 mV and I_s was activated by depolarizing steps from −50 to 70 mV. Currents evoked by voltage steps from −10 to 70 mV are displayed. (*c*) *I-V* relations for I_f (○) and I_s (●) were generated by plotting peak amplitudes against membrane potential.

is illustrated in Fig. 2*c*. In this figure, the τ_{inact} of I_f and I_s are plotted against step potential.

In each case, as the membrane potential approached the voltage at peak amplitude (V_{peak}) for each current, τ_{inact} decreased, indicating an increase in the rate of inactivation. By contrast, at command potentials more positive than V_{peak}, for each current τ_{inact} increased with continued increases in potential. With respect to magnitude, at all potentials τ_{inact} of I_f was significantly faster than that of I_s. For example, τ_{inact} obtained at peak current in 57 cells expressing I_f was 17 ± 0.5 msec, which was significantly faster than τ_{inact} I_s obtained at a peak voltage of I_f (631 ± 102 msec; $n = 33$; $P < 0.001$).

Voltage Dependence of Inactivation

Steady-state inactivation was studied in cells in which only a single type of current (I_f or I_s) was expressed. As shown in Fig. 3*a* and *b*, currents were evoked by applying 5 sec conditioning pulses to the membrane over a range of potentials between −80 and 20 mV, followed by a step depolarization to either 10 mV for I_f(*a*) or 40 mV for I_s(*b*). In Fig. 3*c*, we show the analysis of these two examples. In this figure, current amplitudes, nor-

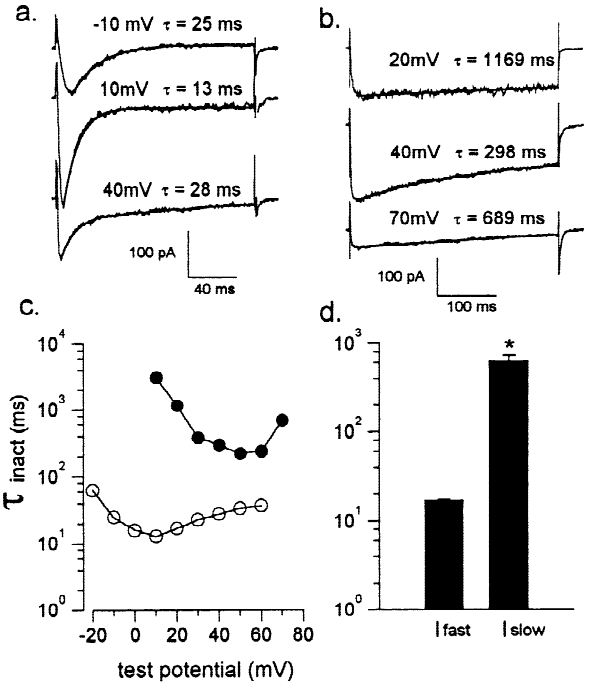

Fig. 2(*a–d*) Time constant of current decay. Current traces in (*a*) and (*b*) were obtained from the cells shown in Fig. 1. The decaying phase of each trace was fitted by a single exponential (*see* text), and the resulting fitted curves (solid lines) were superimposed on the raw traces. Membrane voltage step and time constant for inactivation (τ_{inact}) are shown above each trace. Only three traces are presented for the sake of clarity. (*c*) Relation of τ_{inact} and voltage for I_f (○) and I_s (●). (*d*) Mean τ_{inact} for I_f and I_s obtained for the peak current of each series of recordings. *$P < 0.001$.

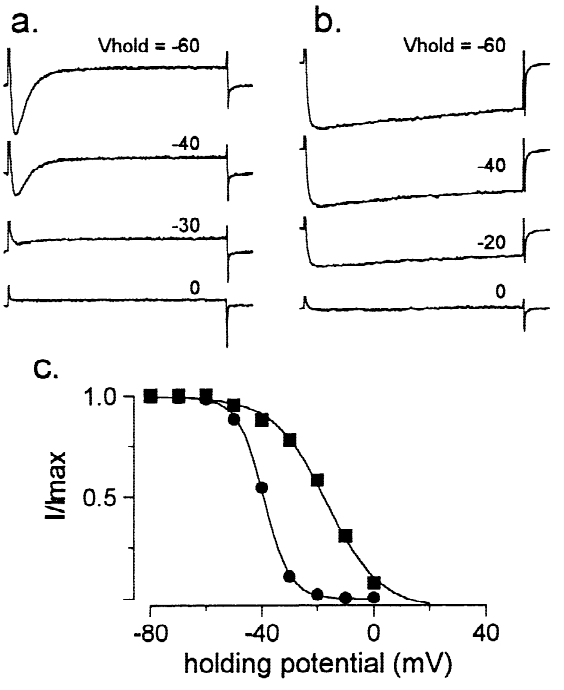

Fig. 3(*a* and *b*) Voltage dependence of steady-state inactivation of I_f and I_s. (*a*) Voltage dependence of steady-state inactivation was determined by measuring peak currents evoked by a single depolarization to either 10 mV for I_f (left column) or 40 mV for I_s (right column) from a range of holding potentials (V_{hold}). (*b*) Steady-state inactivation curves for I_f (●) and I_s (■) were derived by plotting peak currents in (*a*) against V_{hold}, and then fitted by a Boltzmann function (Eq. (2); *see* text). In this example, $V_{1/2}$ was −39 mV for I_f and −17 mV for I_s. Note that at a membrane potential of −30 mV, approximately 90% of I_f was inactivated, compared to only ~20% for I_s.

malized to their peak values, are plotted as a function of conditioning potential.

The resulting curves were fitted with a Voltzmann equation of the following form:

$$I/I_{max} = \{1 + \exp[(V - V_{1/2})/k]\}^{-1} \quad (2)$$

where I/I_{max} is the current magnitude normalized to its maximum value, V represents the conditioning voltage, $V_{1/2}$ the voltage at which I_f or I_s was half-maximum, and k a slope factor which reflects the voltage-sensitivity of steady-state inactivation for the current. In this example, $V_{1/2}$ and k for I_f were −39 mV and −5, respectively, and for I_s, the corresponding values were −17 mV and −9. In general, the steady-state inactivation of I_f occurred at more negative potentials than I_s. For a total of 8 cells with complete records, $V_{1/2}$ and k for I_f were −38 ± 0.8 mV and −4.7 ± 0.2 ($n = 4$), compared to −21 ± 1.1 mV and −11 ± 1.2 for I_s ($n = 4$; $P < 0.002$).

Separation of I_F and I_s

Because I_f inactivated more rapidly than I_s, and the steady-state inactivation potentials for I_f were ~20–30 mV more negative than for I_s, it was possible to separate the two currents by holding cells at specific voltages before depolarizing pulses were applied. An example of such an experiment is shown in Fig. 4. This cell expressed both I_f and I_s when held at −60 mV (Fig. 4*a*). In Fig. 4*c* we plotted peak amplitude (○) and steady-state amplitude (●) *vs.* step voltage for the currents shown in 4*a* to generate two distinct *I-V* curves. Subtracting these two curves generated a third curve, which represented I_f, assuming I_f was completely inactivated by 360 msec. From this hybrid curve (▲), it can be seen that I_f activated at −30 mV and reached peak amplitude at 10 mV. Likewise, the *I-V* curve generated by plotting steady-state values represents I_s, which in this example was activated at −20 mV and reached peak amplitude at 30 mV. By contrast, as shown in Fig. 4*b*, holding the cell at −30 mV effectively inactivated I_f. In this case, *I-V* curves (Fig. 4*d*) generated from peak amplitudes (○) and those measured at 360 msec (●) were virtually identical. In this example, the hybrid curve (▲) revealed only a small inward current.

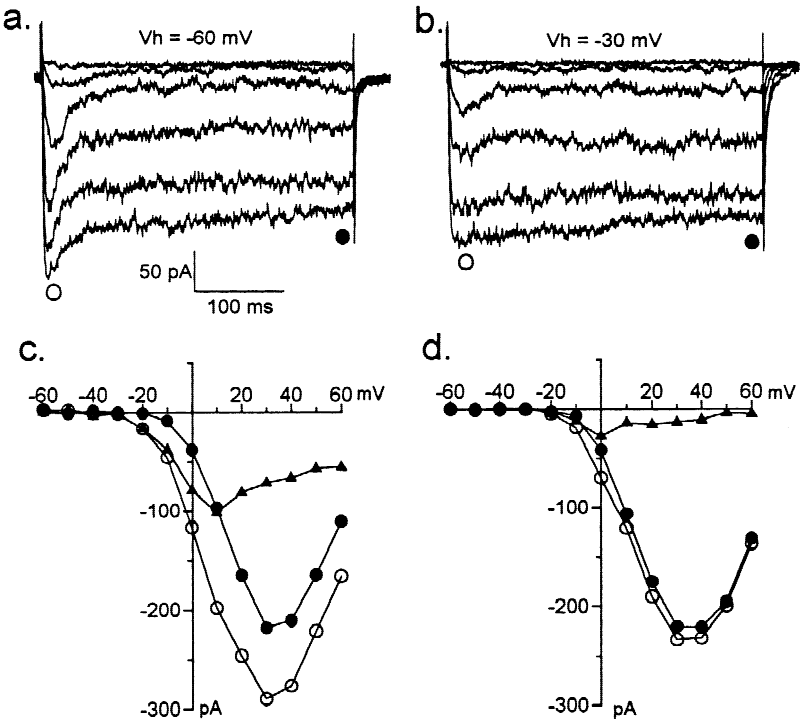

Fig. 4(*a–d*) Separation of I_f and I_s. Family of whole-cell currents obtained from a single cell at a holding potential (V_{hold}) of −60 mV (*a*) or −30 mV (*b*) and evoked by a series of test pulses ranging between −60 to 60 mV. (*c*) *I-V* curves were derived from peak amplitudes (○) and at the end of the 360-msec depolarizing pulses (●) in (*a*). The *I-V* plot representing I_f (▲) was obtained by subtraction (*see* text). Similarly, *I-V* curves in (*d*) were generated using data from (*b*). Note that at a holding potential of −30 mV, I_f (▲) had been effectively inactivated, while I_s (●) remained essentially intact and did not differ from the peak current (○).

Pharmacology of I_F and I_S

Lanthanum (La^{3+}) Blocks Both I_f *and* I_s

To further characterize these currents, we studied the effects of a series of classical Ca^{2+} channel agonists and blockers. Figure 5 illustrates the effects of La^{3+}, a relatively nonspecific Ca^{2+}-channel blocking agent, on I_f(*a*) and I_s(*b*) in two separate cells. From a holding potential of −60 mV, I_f was activated by a depolarizing step to 10 mV, while I_s was activated by a depolarizing step to 30 mV. Under control conditions, these cells were perfused in Ba^{2+}-rich solution, and in each case, either 3 μM or 30 μM $LaCl_3$ was applied to the cell by perfusion. La^{3+} inhibited both I_f and I_s with a similar potency. 3 μM La^{3+} depressed the amplitude of both I_f and I_s by nearly one-half, whereas 30 μM La^{3+} nearly abolished the currents. The effect of La^{3+} is summarized in Fig. 5*c*. In response to 3 μM La^{3+}, the peak amplitude of I_f decreased by 48 ± 6%, from −187 ± 22 pA to −93 ± 10 pA ($n = 10$; $P < 0.005$), and that of I_s decreased 51 ± 5% from −207 ± 32 pA to −96 ± 14 pA ($n = 8$; $P < 0.001$). Likewise, 30 μM La^{3+} reduced I_f by 96 ± 8% to 7.5 ± 5 pA ($P < 0.001$) and I_s by 92 ± 10% to 17 ± 14 pA ($P < 0.005$).

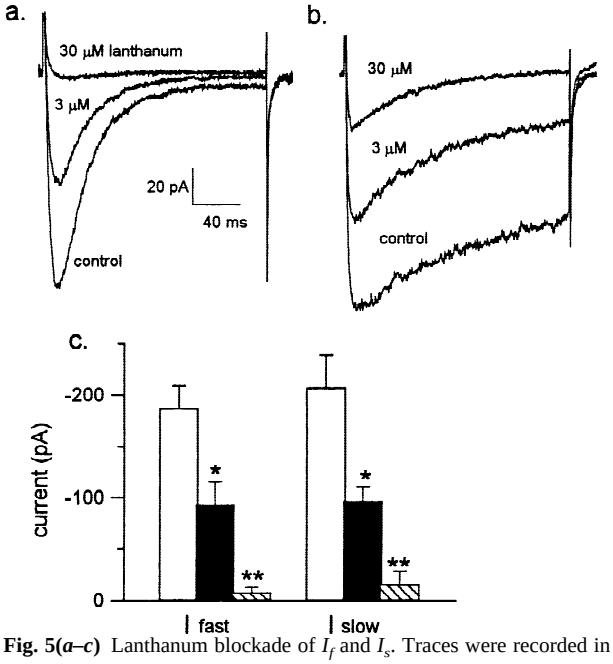

Fig. 5(*a–c*) Lanthanum blockade of I_f and I_s. Traces were recorded in two separate pulp cells. (*a*) Lanthanum blocks I_f activated by depolarizing steps to 10 mV from a holding potential of −60 mV. (*b*) Lanthanum blocks I_s evoked by step depolarizations to 40 mV. (*c*) Mean peak current for I_f (right panel; $n = 10$) and I_s (left panel; $n = 8$) in control conditions (open bar), 3 μM La^{3+} (filled bar) or 30 μM La^{3+} (cross-hatching). *$P < 0.005$; **$P < 0.001$.

Nifedipine and Bay-K Affect I_s *but not* I_f

The effect of Bay-K and nifedipine on the two currents are shown in Fig. 6*a* and *b*. As described above, cells were first perfused with a Ba^{2+}-rich solution, and from a holding potential of −60 mV, I_f was activated by a depolarizing step to 10 mV and I_s was activated by a depolarizing step to 30 mV. The bath solution was then changed to one containing either 5 μM Bay-K or 10 μM

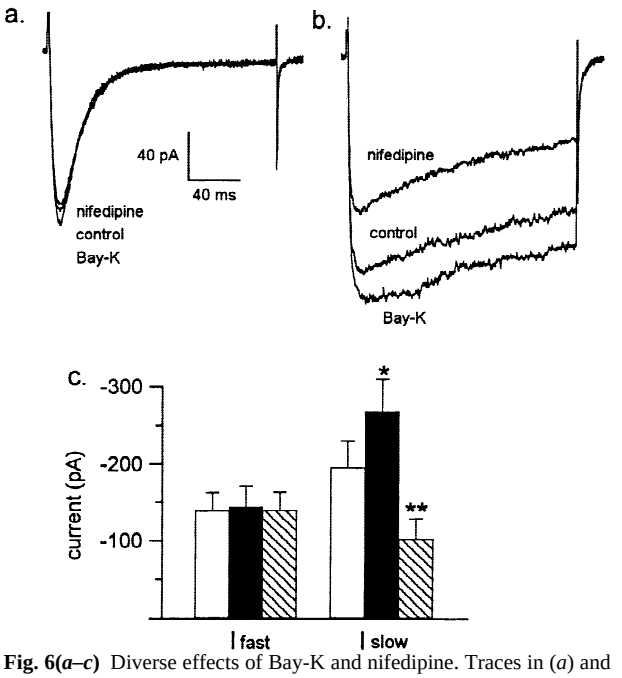

Fig. 6(*a–c*) Diverse effects of Bay-K and nifedipine. Traces in (*a*) and (*b*) were activated by depolarizing steps to 10 and 40 mV, respectively, under control conditions, in the presence of 5 μM Bay-K or 10 μM nifedipine. (*c*) Mean peak amplitudes for I_f ($n = 7$) and I_s ($n = 11$) obtained under control conditions (open bar) and in the presence of Bay-K (filled bar) or nifedipine (crosshatching). *$P < 0.03$; **$P < 0.005$.

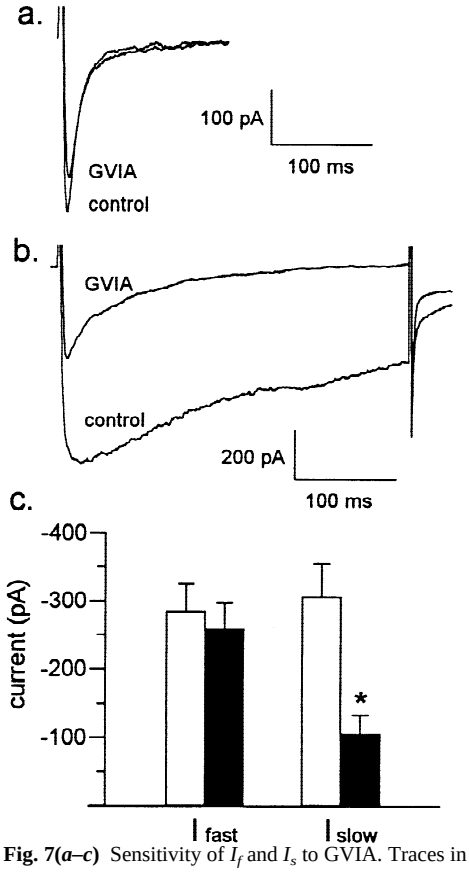

Fig. 7(*a–c*) Sensitivity of I_f and I_s to GVIA. Traces in (*a*) and (*b*) were evoked by 360-msec depolarizing steps to either 10 mV (*a*) or 20 mV (*b*) from a holding potential of −60 mV. Compared to control, 2 μM GVIA blocked I_s but not I_f. (*c*) Summary histograms. For I_f, peak amplitude did not differ between control (open bar) and GVIA (filled bar; $P > 0.6$). By contrast, GVIA significantly reduced peak amplitude of I_s by ~66%. *$P < 0.006$.

nifedipine. As shown in Fig. 6*a*, I_f was insensitive to both Bay-K and nifedipine, whereas I_f was enhanced by Bay-K and depressed by nifedipine (Fig. 6*b*). The effects of Bay-K and nifedipine on I_f ($n = 7$) and I_s ($n = 11$) are summarized in Fig. 6*c*. Peak amplitude for I_f under control conditions was −138 ± 24 pA *vs.* −144 ± 27 pA ($P > 0.2$) in the presence of 5 μM Bay-K, or −139 ± 24 pA ($P > 0.2$) in the presence of 10 μM nifedipine. By contrast, in response to 5 μM Bay-K, I_s increased ~37%, from −195 ± 35 pA to −268 ± 42 pA ($P < 0.003$), while 10 μM nifedipine reduced peak amplitude ~62%, from −268 ± 42 pA to −102 ± 66 pA. In general, these results clearly suggested that I_f and I_s were mediated by different Ca^{2+} channels, and in particular, that I_s contained at least a dihydropyridine-sensitive component, namely, a conductance mediated by L-type Ca^{2+} channels.

GVIA Affects I_s *but not* I_f

We then examined the sensitivity of I_f and I_s to the peptide omega-Conotoxin GVIA (GVIA), a predominantly N-type calcium channel blocker from the cone shell *Conus geographus* [12]. After control peak currents were obtained as described above, 2 μM GVIA was applied to the bath by perfusion. As shown in Fig. 7*a* and *b*, I_f was largely insensitive to GVIA, whereas I_s was significantly inhibited. Summary data for this experiment is shown in Fig. 7*c*. There was a negligible effect of GVIA on I_f ($n = 9$). For this current, GVIA reduced peak amplitude from −284 ± 41 pA to −258 ± 49 pA ($P > 0.6$). By contrast, GVIA decreased the peak amplitude of I_s by ~66%, from −306 ± 59 pA to −105 ± 28 pA ($n = 9$; $P < 0.006$). This result further confirmed that I_f and I_s were carried by different Ca^{2+} channels, and strongly suggested that I_s was also mediated by an N-type Ca^{2+} channel.

As both nifedipine and GVIA, when applied separately, significantly blocked I_s but had no effect on I_f in cells which displayed predominantly a single current type (Figs. 6 and 7), we further tested whether nifedipine and GVIA had the same effect on I_f and I_s from cells expressing both of these current types. One such example is shown in Fig. 8. In Fig. 8*a* we show the family of currents evoked by a series of 160-msec depolarizing pulses, from −60 to 60 mV, for control conditions (left panel), in the presence of GVIA (middle panel), and in

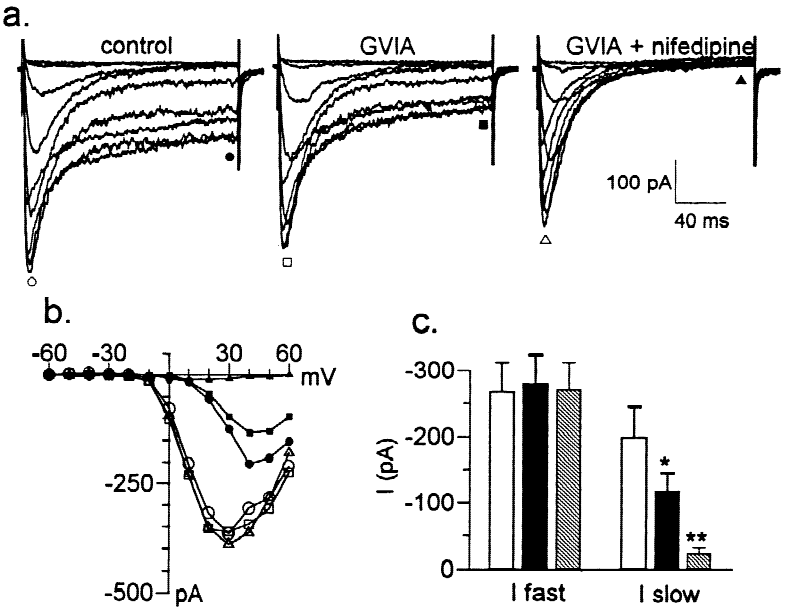

Fig. 8(*a–c*) Effects of GVIA and nifedipine for cells expressing both I_f and I_s. (*a*) Family of currents evoked by 160-msec depolarizing pulses from −20 to 60 mV from a holding potential of −60 mV obtained in 110 mM $BaCl_2$ (left panel; "control"), in the presence of 2 μM GVIA (middle panel; GVIA), and with both 2 μM GVIA and 10 μM nifedipine (right panel; GVIA + nifedipine) in the external bath. The open and filled symbols represent peak and steady-state amplitudes, respectively. (*b*) *I-V* relations were obtained by plotting peak amplitudes (I_f; open symbols), derived by subtracting the steady-state amplitude from the evoked peak, or steady-state amplitudes (I_s; filled symbols) for the traces in (*a*) as a function of test potential. For peak current (○), compared to control conditions I_f was unaffected by either GVIA (□) or GVIA supplemented by nifedipine (△). By contrast, for steady-state current (●), I_s was partially blocked by GVIA alone (■), and completely blocked by a combination of GVIA and nifedipine (▲). (*c*) Summary histograms representing the amplitudes of I_f (left panel) and I_s (right panel) for a total of 6 cells recorded in 110 mM $BaCl_2$ (open bar), or after exposure to GVIA (filled bar), or GVIA plus nifedipine (crosshatching). $*P < 0.014$; $**P < 0.005$.

the presence of both GVIA and nifedipine (right panel). Figure 8*b* shows the *I-V* relations for these currents, for both I_s, represented by the steady-state amplitude measured at the end of each pulse (filled symbols), and I_f, generated by subtracting the peak amplitude (open symbols) from that of the steady-state. In 110 mM $BaCl_2$ bath solution, I_s (●) was activated at 10 mV and reached peak amplitude (−204 pA) at 40 mV, whereas I_f (○) was activated at −10 mV and reached a peak amplitude of −366 pA at 30 mV. By contrast, in the presence of 2 μM GVIA, I_s (■) decreased by 71 pA, to −133 pA, while I_f (□) was virtually unchanged. The subsequent perfusion of the cell with 2 μM GVIA and 10 μM nifedipine further decreased I_s (▲) by 122 pA, to −11 pA, while I_f (△) was unaffected. Summary data for 6 cells that displayed both I_f and I_s are shown in Fig. 8*c*. I_f was effectively insensitive to both GVIA and nifedipine. The averaged amplitude was −268 ± 44 pA in the control condition (open), −281 ± 43 pA when exposed to GVIA (filled), and −271 ± 41 when exposed to both GVIA and nifedipine (cross-hatch). None of these amplitudes differed significantly (ANOVA; $P > 0.05$). By contrast, I_s was sensitive to both GVIA and nifedipine: 2 μM GVIA blocked approximately 41% of I_s, reducing its amplitude to −118 ± 27 from −199 ± 47 pA ($P < 0.014$), and exposing cells to 10 μM nifedipine in addition to GVIA further reduced the current by ~80%, from −118 ± 27 to −23 ± 9 pA ($P < 0.005$). These results were consistent with those obtained from cells predominantly expressing either I_f or I_s (*see* Fig. 7), further suggesting that I_s was mediated by both GVIA and nifedipine-sensitive conductances, and that these conductances could co-exist in a single cell.

Activation of Na^+ and Ca^{2+} Currents

When cells were perfused with a standard Na^{2+}-rich solution, and recording pipettes were filled with CsCl, a voltage-gated inward current could occasionally be detected. This inward current consisted of two components, with fast and slow activation and inactivation kinetics, respectively. The fast component could be abolished by 2 μM TTX, while the slow component unaffected by TTX, was completely abolished by 100 μM La^{3+}. One such example of this phenomenon is shown in Figs. 9*a* and *b*. It should be noted that when compared to the majority of cells (*see* below), this appeared to be a uniquely large Ca^{2+} current. These results confirmed the existence of a voltage-gated, TTX-sensitive Na^+ current in mammalian pulp cells, as we had previously described in primary cultures derived from human dental pulp [5], and demonstrated again, that the slow component was mediated by Ca^{2+} channels.

To further characterize the Ca^{2+} current, additional experiments were conducted in standard Na^+-rich solution containing 2 mM Ca^{2+} and 2 μM TTX. For 37 cells tested, 34% (14/34) displayed a detectable inward Ca^{2+} current under these conditions, with a mean peak amplitude of −60 ± 9 pA. Increasing bath Ca^{2+} from 2 to 5 mM

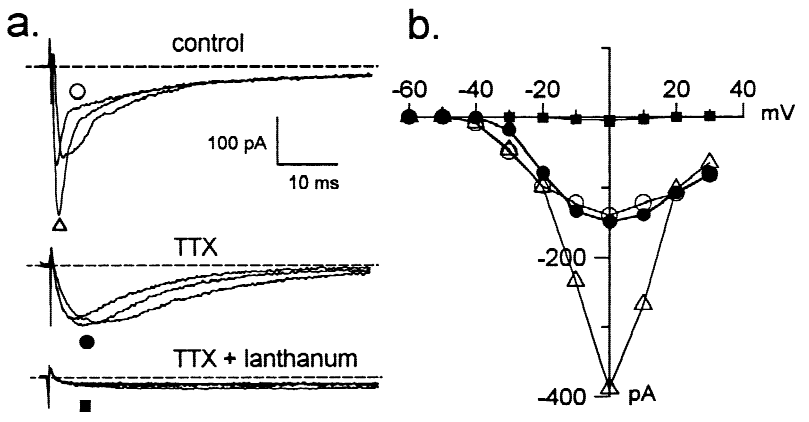

Fig. 9(*a* and *b*) Voltage-gated Na^+ and Ca^{2+} currents. This cell was perfused with Na^+-rich saline containing 2 mM Ca^{2+}. (*a*) From a holding potential of −80 mV, whole-cell currents were evoked by 60-msec depolarizing pulses to voltage steps ranging from −60 to 30 mV. Only traces from −10, 0 and 10 mV are shown. The inward current contained two components, with both fast and slow kinetics (upper panel). The fast component was abolished by 2 μM TTX (middle panel), and the slow component was effectively blocked by 100 μM La^{3+} (lower panel). (*b*) *I-V* relation of peak amplitude of the fast (△) and slow (○) components in the control conditions, and in the presence of TTX (●) or TTX and La^{3+} (■).

significantly increased the magnitude of the Ca^{2+} current by ~2.3-fold, to −137 ± 16 pA ($P < 0.0002$), and subsequent addition of 0.2 mM La^{3+} completely blocked it. A typical example of one of these experiments is shown in Fig. 10. In this example, from a holding potential of −60 mV, inward current was evoked every 3 sec by a depolarizing step to 10 mV. With 2 mM Ca^{2+} in the bath, the amplitude was ~−20 pA, which increased to a peak of −145 pA with the addition of 3 mM Ca^{2+}. The current reached a steady-state amplitude of −90 pA, and could be blocked by adding 0.2 mM La^{3+} to the bath. Interestingly, for 8/11 cells in which no detectable Ca^{2+} current was observed, Ca^{2+} currents appeared after following the addition of 3 mM Ca^{2+} into bath. Taken together, these results suggested that in dental pulp cells, both amplitude and incidence of Ca^{2+} currents were largely dependent on external Ca^{2+} concentration.

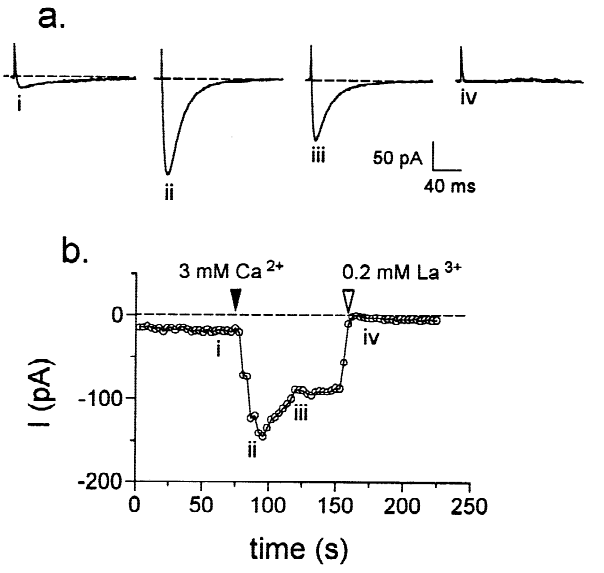

Fig. 10 (*a* and *b*) Enhancement of Ca^{2+} current by external Ca^{2+} and blockade by La^{3+}. (*a*) Traces were induced by depolarizing steps 10 mV applied to the cell every 3 sec, and recorded under control conditions (i), following addition of 3 mM Ca^{2+} to the bath (ii, iii), and (iv), after application of 0.2 mM La^{3+}. (*b*) Time course of peak inward currents. Open circles represent peak amplitudes plotted at 0.33 Hz. Numerals [i–iv] correspond to representative traces in (*a*). Filled and open arrows indicate application of Ca^{2+} and La^{3+} to the bath. Dashed lines represent zero-current levels.

Discussion

We have identified two classes of inward Ba^{2+} current, I_f and I_s, in a distinct subpopulation of fibroblasts found in 1st–2nd passage primary cultures derived from rat dental pulp. These two currents were mediated by distinct classes of Ca^{2+} channel based on voltage-dependent inactivation kinetics and sensitivity to specific Ca^{2+} channel agonists and blocking agents. I_f currents displayed voltage-dependent, fast activation and inactivation kinetics, while I_s inactivated more slowly (Fig. 1). The inactivation time-constant (τ_{inact}) of I_s was nearly 40-fold greater than that of I_f. In addition, both the threshold activation as well as peak activation potentials of I_f were ~20–40 mV more negative than those of I_s (Fig. 2). Analysis of steady-state activation and inactivation of I_f and I_s also revealed that relative to those of I_s, all voltage-dependent properties I_f were shifted ~20–40 mV towards more negative potentials. The gating kinetics of I_f and I_s are consistent with those of low voltage-activated (LVA) and high voltage-activated (HVA) conductances, in particular, T- and L-type Ca^{2+} currents, observed in a number of other cell types [14, 25].

I_f currents were the predominant class in 52% of dental pulp cells, while I_s predominated in 31% of these cells. In the remaining 17% of the cells, both I_f and I_s could be observed. In general, I_s could be isolated from I_f by holding the cell at membrane potentials more positive than −30 mV, since ~87% of I_f was inactivated and only 22% of I_s was inactivated at that holding potential (Figs. 3 and 4). This result strongly confirmed that I_f and I_s were mediated by different classes of Ca^{2+} channel.

The pharmacology of I_f and I_s further confirmed that they represented different channels. Not surprisingly, both I_f and I_s showed high sensitivity to La^{3+}, a nonspecific Ca^{2+} channel blocking agent [21, 26], which depressed I_f and I_s almost equally. I_s was significantly enhanced by Bay-K, a specific activator of L-type Ca^{2+} channels [13, 32] and inhibited by nifedipine, a specific blocker of L-type Ca^{2+} channels [14]. By contrast, I_f was unaffected by either of these two dihydropyridine derivatives. Furthermore, I_f was insensitive to blockade by GVIA, a specific blocker of N-type Ca^{2+} channel [10, 34], while 40 ~ 60% of I_s was reduced by this peptide (Figs. 7 and 8). These findings suggest that I_s was mediated by *both* dihydropyridine-sensitive L-type and GVIA-sensitive N-type Ca^{2+} channels. Because N-type Ca^{2+} channel may also display sustained, noninactivating channel activity [2, 29], a characteristic property of L-type Ca^{2+} channels, in this study these two components could not be discriminated by their activation and inactivation kinetics alone.

The existence of N-type Ca^{2+} channels in the dental pulp fibroblast probably reflects its neural-crest origin, since N-type channels are thought to be expressed predominately in neuronal tissue [3, 7] and N-type Ca^{2+} channels have not been found in either fibroblasts [11, 28], or bone-forming cells [8]. In addition, we observed a prominent voltage-gated, rapidly inactivating inward Na^+ current in these cells (Fig. 9), confirming our previous studies in human dental pulp [5]. In these experiments, isolation of Ca^{2+} current from Na^+ current could be achieved using micromolar application of TTX [17, 30].

In mammalian dental pulp, undifferentiated fibroblastic cells are thought to have the capacity to differentiate into odontoblast-like cells and form mineral, i.e., dentin, as a protective response to injury [1, 19, 20, 27, 31, 33]. For presumptive mineral-inductive cells such as these, calcium embodies a critical extra- and intracellular signal during the process of mineral formation, and while exact mechanisms remain unclear, calcium mobilization and transport are fundamental to this process [18, 35]. Thus, the existence of two very prominent Ca^{2+} conductances in these cells, which allows for influx of external Ca^{2+} over a wide range of membrane potential and with an equally broad temporal spectrum, is consistent with a putative role during reparative dentin formation in mammalian dental pulp.

This research was supported by NIH-NIDCR Grant DE11651 to RMD.

References

1. Bouvier, M., Joffre, A., Magloire, H. 1990. In vitro mineralization of a three-dimensional collagen matrix by human dental pulp cells in the presence of chondroitin sulfate. *Arch. Oral Biol.* **35:**301–309
2. Carbone, E., Sher, E., Clementi, F. 1990. Ca currents in human neuroblastoma IMR32 cells: kinetics, permeability and pharmacology. *Pfluegers Arch.* **416:**170–179
3. Cruz, L.J., Johnson, D.S., Olivera, B.M. 1987. Characterization of the omega-Conotoxin target. Evidence for tissue-specific heterogeneity in calcium channel types. *Biochemistry* **26:**820–824
4. Davidson, R.M. 1993. Potassium currents in cells derived from human dental pulp. *Arch. Oral Biol.* **38:**803–811
5. Davidson, R.M. 1994. Neural form of voltage-dependent sodium current in human cultured dental pulp cells. *Arch. Oral Biol.* **39:**613–620
6. Denis, I., Pointillart, A., Lieberherr, M. 1994. Effects of growth hormone and insulin-like growth factor-I on the proliferation and differentiation of cultured pig bone cells and rat calvaria cells. *Growth Regul.* **4:**123–130
7. Dubel, S.J., Starr, T.V., Hell, J., Ahlijanian, M.K., Enyeart, J.J., Catterall, W.A., Snutch, T.P. 1992. Molecular cloning of the alpha-1 subunit of an omega-Conotoxin-sensitive calcium channel. *Proc. Natl. Acad. Sci. USA* **89:**5058–5062
8. Duncan, R.L, Akanbi, K.A., Farach-Carson, M.C. 1998. Calcium signals and calcium channels in osteoblastic cells. *Semin Nephrol.* **18:**178–190
9. Eklou-Kalonji, E., Denis, I., Lieberherr, M., Pointillart, A. 1998. Effects of extracellular calcium on the proliferation and differentiation of porcine osteoblasts in vitro. *Cell Tissue Res.* **29:**163–171
10. Ellinor, P.T., Zhang, J.F., Horne, W.A., Tsien, R.W. 1994. Structural determinants of the blockade of N-type calcium channels by a peptide neurotoxin. *Nature* **372:**272–275
11. Estacion, M. 1991. Characterization of ion channels seen in subconfluent human dermal fibroblasts. *J. Physiol.* **436:**579–601
12. Flinn, J.P., Pallaghy, P.K., Lew, M.J., Murphy, R., Angus, J.A., Norton, R.S. 1999. Role of disulfide bridges in the folding, structure and biological activity of omega-Conotoxin GVIA. *Biochim. Biophys. Acta* **1434:**177–190
13. Fox, A.P., Nowycky, M.C., Tsien, R.W. 1987. Kinetic and pharmacological properties distinguishing three types of calcium currents in chick sensory neurones. *J. Physiol.* **394:**149–172
14. Fox, A.P., Nowycky, M.C., Tsien, R.W. 1987. Single-channel recordings of three types of calcium channels in chick sensory neurones. *J. Physiol.* **394:**173–200
15. Guo, L., Davidson, R.M. 1998. Potassium and chloride channels in freshly isolated rat odontoblasts. *J. Dent. Res.* **77:**341–350
16. Guo, L., Davidson, R.M. 1999. Extracellular Ca^{2+} increases cytosolic free Ca^{2+} in freshly isolated rat odontoblasts. *J. Bone Miner. Res.* **14:**1357–1366
17. Kao, C.Y. 1981. Tetrodotoxin, saxitoxin, chiriquitoxin: new perspectives on ionic channels. *Fed. Proc.* **40:**30–35
18. Kardos, T.B., Hunter, A.R., Hanlin, S.M., Kirk, E.E. 1998. Odontoblast differentiation: a response to environmental calcium? *Endod. Dent. Traumatol.* **14:**105–111
19. Kasugai, S., Adachi, M., Ogura, H. 1988. Establishment and characterization of a clonal cell line (RPC-C2A) from dental pulp of the rat incisor. *Arch. Oral Biol.* **33:**887–891
20. Kitamura, C., Kimura, K., Nakayama, T., Terashita, M. 1999. Temporal and spatial expression of c-jun and jun-B protooncogenes in pulp cells involved with reparative dentinogenesis after cavity preparation of rat molars. *J. Dent. Res.* **78:**673–680
21. Lewis, B.D., Spalding, E.P. 1998. Nonselective block by La^{3+} of *Arabidopsis* ion channels involved in signal transduction. *J. Membrane Biol.* **162:**81–90
22. Linde, A., Goldberg, M. 1993. Dentinogenesis. *Crit. Rev. Oral Biol. Med.* **4:**679–728

23. Linde, A., Lundgren, T. 1990. Calcium transport in dentinogenesis. *J. Biol. Buccale* **18:**155–160
24. Nakashima, M. 1991. Establishment of primary cultures of pulp cells from bovine permanent incisors. *Arch. Oral Biol.* **36:**655–663
25. Narahashi, T., Tsunoo, A., Hoshii, M. 1987. Characterization of two types of calcium channels in mouse neuroblastoma cells. *J. Physiol.* **383:**231–249
26. Nathan, R.D., Kanai, K., Clark, R.B., Giles, W. 1988. Selective block of calcium current by lanthanum in single bullfrog atrial cells. *J. Gen. Physiol.* **91:**549–572
27. Onishi, T., Kinoshita, S., Shintani, S., Sobue, S., Ooshima, T. 1999. Stimulation of proliferation and differentiation of dog dental pulp cells in serum-free culture medium by insulinlike growth factor. *Arch. Oral Biol.* **44:**361–371
28. Peres, A., Sturani, E., Zippel, R. 1988. Properties of the voltage-dependent calcium channel of mouse Swiss 3T3 fibroblasts. *J. Physiol.* **401:**639–655
29. Plummer, M.R., Hess, P. 1991. Reversible uncoupling of inactivation in N-type calcium channels. *Nature* **351:**657–659
30. Romey, G., Abita, J.P., Schweitz, H., Wunderer, G., Lazdunski, M. 1976. Sea anemone toxin: a tool to study molecular mechanisms of nerve conduction and excitation-secretion coupling. *Proc. Natl. Acad. Sci. USA* **73:**4055–4056
31. Ruch, J.V. 1998. Odontoblast commitment and differentiation. *Biochem. Cell Biol.* **76:**923–938
32. Scott, R.H., Dolphin, A.C. 1988. The agonist effect of Bay K 8644 on neuronal calcium channel currents is promoted by G-protein inactivation. *Neurosci. Lett.* **89:**170–175
33. Seux, D., Couble, M.L., Hartmann, D.J., Gauthier, J.P., Magloire, H. 1991. Odontoblast-like cytodifferentiation of human dental pulp cells in vitro in the presence of a calcium hydroxide-containing cement. *Arch. Oral Biol.* **36:**117–128
34. Williams, M.E., Brust, P.F., Feldman, D.H., Patthi, S., Simerson, S., Maroufi, A., McCue, A.F., Velicelebi, G., Ellis, S.B., Harpold, M.M. 1992. Structure and functional expression of an omega-Conotoxin-sensitive human N-type calcium channel. *Science* **257:**389–395
35. Yoshiba, K., Yoshiba, N., Nakamura, H., Iwaku, M., Ozawa, H. 1996. Immunolocalization of fibronectin during reparative dentinogenesis in human teeth after pulp capping with calcium hydroxide. *J. Dent. Res.* **75:**1590–1597